Journal of Power Sources 184 (2008) 180–190

Contents lists available at ScienceDirect

Journal of Power Sources

journal homepage: www.elsevier.com/locate/jpowsour

Characterization of a liquid feed direct methanol fuel cell with Sierpinski carpets fractal current collectors

Jing-Yi Chang [a], Yean-Der Kuan [b,*], Shi-Min Lee [c], Shah-Rong Lee [d]

[a] Department of Mechanical and Electro-Mechanical Engineering, Tamkang University, Tamsui, 251 Taipei County, Taiwan, ROC
[b] Department of Refrigeration, Air Conditioning and Energy Engineering, National Chin-Yi University of Technology, No. 35, Lane 215, Section 1, Chung-Shan Road, Taiping City, Taichung County, 411 Taiwan, ROC
[c] Department of Aerospace Engineering, Tamkang University, Tamsui, 251 Taipei County, Taiwan, ROC
[d] Department of Mechanical Engineering, Technology and Science Institute of Northern Taiwan, Peitou, 112 Taipei, Taiwan, ROC

ARTICLE INFO

Article history:
Received 10 April 2008
Received in revised form 4 June 2008
Accepted 5 June 2008
Available online 20 June 2008

Keywords:
Fractal
Current collector
Direct methanol fuel cell
DMFC

ABSTRACT

The bipolar plate/current collector plays an important role in direct methanol fuel cells (DMFC). A current collector with different geometries could have a significant influence on cell performance. This paper presents fractal geometry application to current collector design in a direct methanol fuel cell (DMFC). This new current collector design is named CCFG (Current Collectors with Fractal Geometry). This research determined how to make a better free open design for the current collector on a printed circuit board based DMFC. The results show that both the free area ratio and total holes perimeter length on the bipolar plate affect the cell performance. The total number of holes on the perimeter presents greater effects than the free open ratio. The cell performance is more sensitive using a cathode current collector than the anode current collector.

1. Introduction

In recent years studies on substitute energies have rapidly increased. The fuel cell is one of the most attractive power sources for the new generation technology. It is an electrochemical device that converts the chemical energy from a chemical reaction directly into high efficiency electrical energy [1]. Among the different types of fuel cells, the direct methanol fuel cell (DMFC) is considered the most promising power source for cell phones, small portable generators and automobile applications. The fuel cell has these important advantages, relatively mild operating conditions (low temperature and pressure operations), fast and convenient refueling, easy liquid fuel storage, low cost methanol, relatively hydrogen-dense, natural gas usable, converting methanol directly into electricity without a bulkley reformer in the middle and ready for compact design [2].

A DMFC uses either vapor or liquid methanol as fuel and operates at relatively low temperature. The cell reaction takes place at the anode and cathode. The reactions are as follows [3].

$$\text{Anode}: \quad CH_3OH + H_2O \rightarrow 6e^- + 6H^+ + CO_2 \tag{1}$$

$$\text{Cathode}: \quad \frac{3}{2}O_2 + 6e^- + 6H^+ \rightarrow 3H_2O \tag{2}$$

$$\text{Overall}: \quad CH_3OH + \frac{3}{2}O_2 \rightarrow 2H_2O + CO_2 \tag{3}$$

Methanol and water are converted into carbon dioxide, protons and electrons at the anode side. The hydrogen protons are transported to the cathode through a polymer electrolyte membrane and the electrons are transported through the external circuit. The protons and electrons reduce oxygen to form water at the cathode side. To evaluate the performance of a fuel cell, the classical experiment is conducted to measure the stationary current–voltage characteristics. The characteristic curve (I–V curve) reflects the different limiting mechanism occurring during fuel cell operation at zero current, low current density, and high current voltage. The open circuit voltage depends on the methanol concentration. The cell performance is influenced mainly by the reaction kinetic limitation in the low current density range and the mass transport limitation in the high current density range [3].

A traditional single DMFC structure is shown in Fig. 1. The anode and cathode polar plates are made of graphite or metal. The flow channels inside the polar plates are grooved. The anode and cathode polar plates play the role of both fuel distribution and electrical collection. However, the planar type DMFCs with multiple cells appear increasingly in demand because they are

* Corresponding author. Tel.: +886 4 23924505x8256; fax: +886 4 23932758.
E-mail address: ydkuan@ncut.edu.tw (Y.-D. Kuan).

0378-7753/$ – see front matter © 2008 Elsevier B.V. All rights reserved.
doi:10.1016/j.jpowsour.2008.06.024

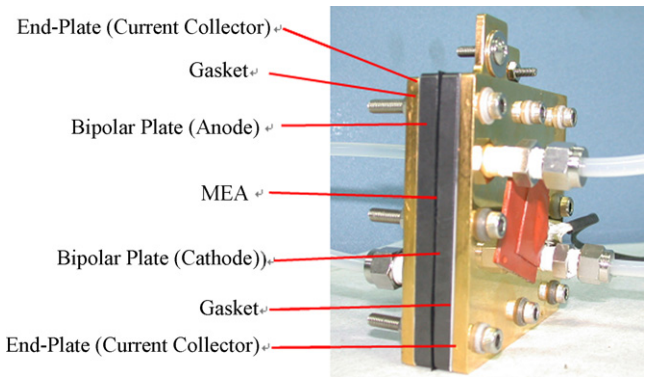

Fig. 1. Traditional DMFC structure.

more flexible in design and application. A planar printed-circuit-board fuel cell (PCB DMFC) module with separate flow channel and electrical collection is shown in Fig. 2. The open hole ratio and the size and type of holes in the electric collector which differ in the perimeter holes density are important issues in DMFC performance.

The bipolar plate is a significant part of the PEMFC and DMFC stacks. In a typical PEM or DMFC fuel cell, the bipolar plate functions include carrying current away from the cell, distributing the fuel and oxidant within the cell, facilitating water and thermal management and separating individual cells in the stack. The bipolar plate materials much possess high electrical and thermal conductivity, good corrosion resistance, sufficient compressive strength and low density [4–6]. The current collectors presented in this paper were produced using fractal geometry, called CCFG (current collector with fractal geometry).

The fractal geometry theory was proposed by Mandelbrot [7] and is mathematically defined in the "Haussdorff dimensions," which are a set of non-integers. The main characteristics of a fractal pattern are self-similarity, sub-divisibility and recursive nature. The theory describes certain phenomena that are difficult to describe in very fine variations using convectional methods such as the contour of seashores, the slopes of valleys or patterns of clouds. The fractal theory has been applied in many engineering fields such as the variations in entropy and heat transfer by Lee and Lin [8], tree network for electronic cooling application by Bejan and co-workers [9], cooling of a circular heated surface using fractal-like branching channel networks by Pence [10], fractal generation for heat sink fins by Lee et al. [11] and an automatic polishing path by Chen et al. [12].

Tüber et al. [13] presented fractal structures as flow fields in PEMFCs and DMFCs for portable applications. They applied "Frac-Therm" theory, which was originally generated to design structures for heat-exchangers and fractal structures for a DMFC flow field on the bipolar plates. A multiple-branched structure with smooth flow path similar to biological fluid channels was adopted in their

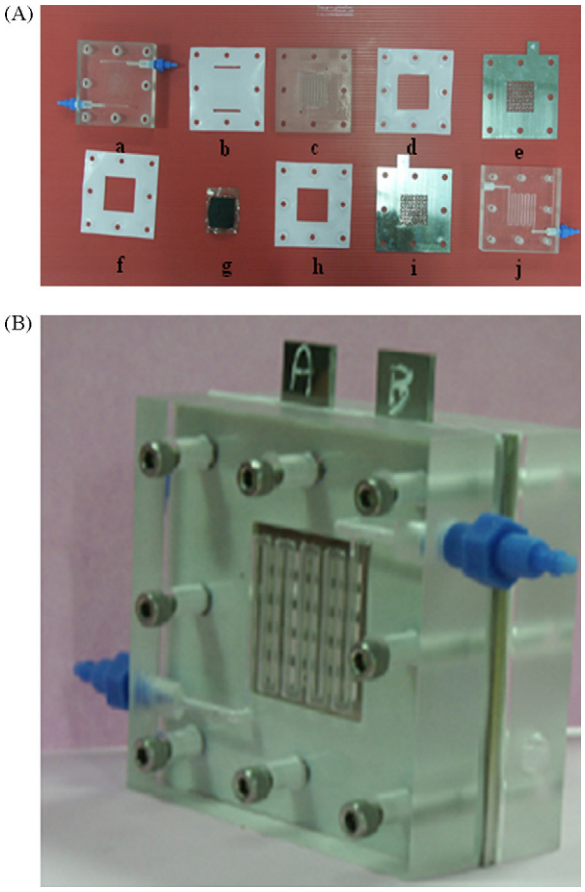

Fig. 3. Construction of the single cell DMFC fixture. (A) DMFC components. (a) Anode inlet/outlet flow board, (b) Gasket, (c) Anode flow board, (d) Gasket, (e) Anode current collector, (f) Gasket, (g) MEA, (h) Gasket, (i) Cathode current collector and (j) Cathode airflow board. (B) DMFC Assembly.

research and compared with serpentine and parallel flow fields. Their results showed that a serpentine flow channel has better cell stability and performance but much more pressure drop across the channel. Both multiple-branched fractal and parallel flow fields could be alternate structures with lower pressure drop with similar performance. Moreover, they found that the lower pressure loss in the fractal flow field decreases the parasitic energy demand and achieves a more homogeneous flow distribution compared with a parallel design.

However, no further discussion on the fractal theory was applied to fuel cells in the literature even though fractal theory is generates systemic geometry. This paper will apply the Sierpinski carpet [14,15] fractal geometry to design DMFC current collectors. Two important factors are involved: the open ratio and perimeter length of the holes.

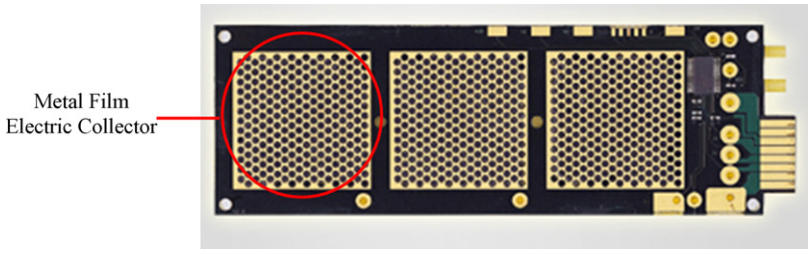

Fig. 2. Planar PCB-package DMFC module.

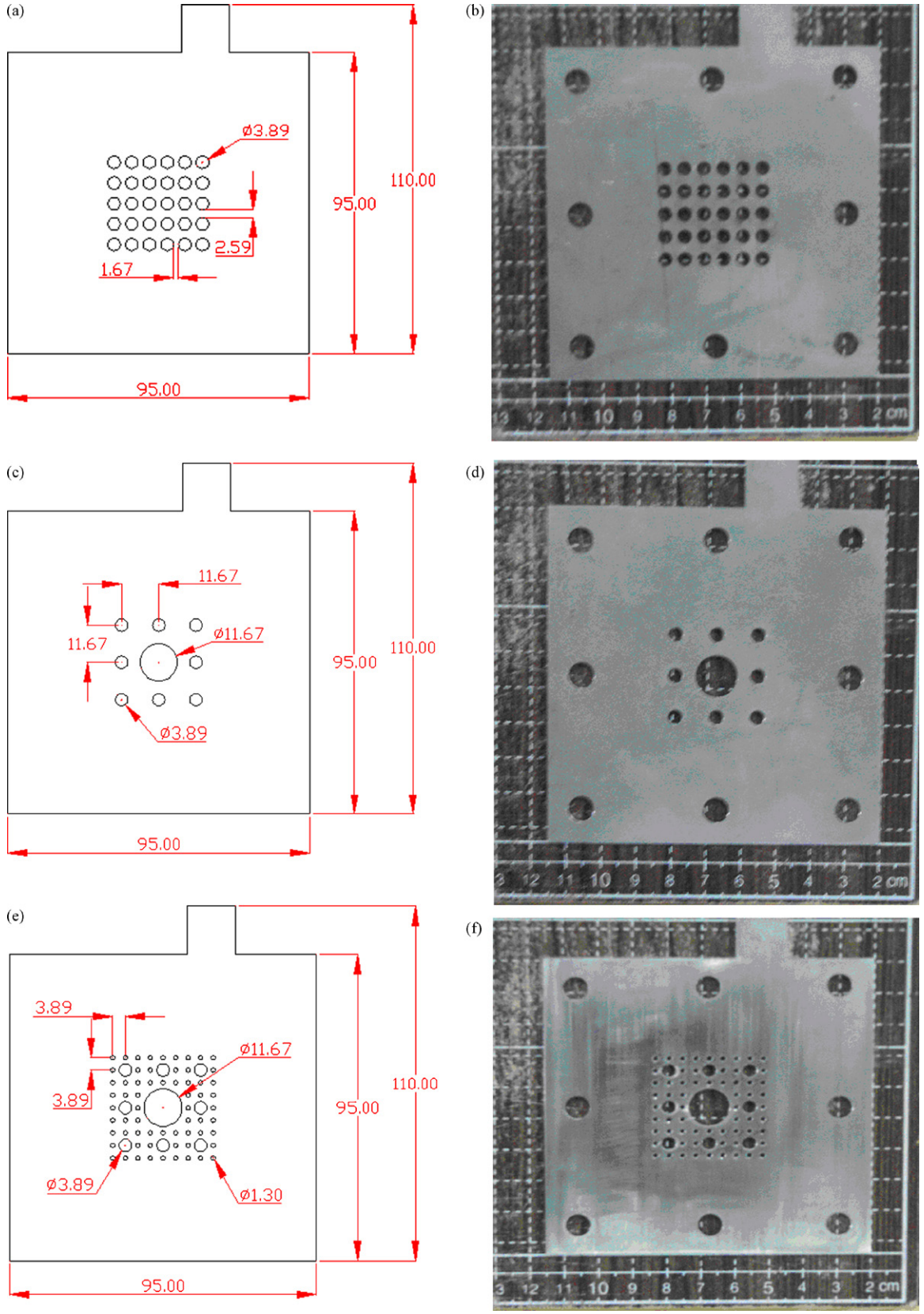

Fig. 4. Circular standard and Sirpsiski carpet fractal current collectors. (a) Standard circular current collector (SCCC). (b) Picture of SCCC. (c) 1st order circular fractal current collector (CFCC1). (d) Picture of CFCC1. (e) 2nd order Sirpsiski carpet circular current collector (CFCC2). (f) Picture of CFCC2.

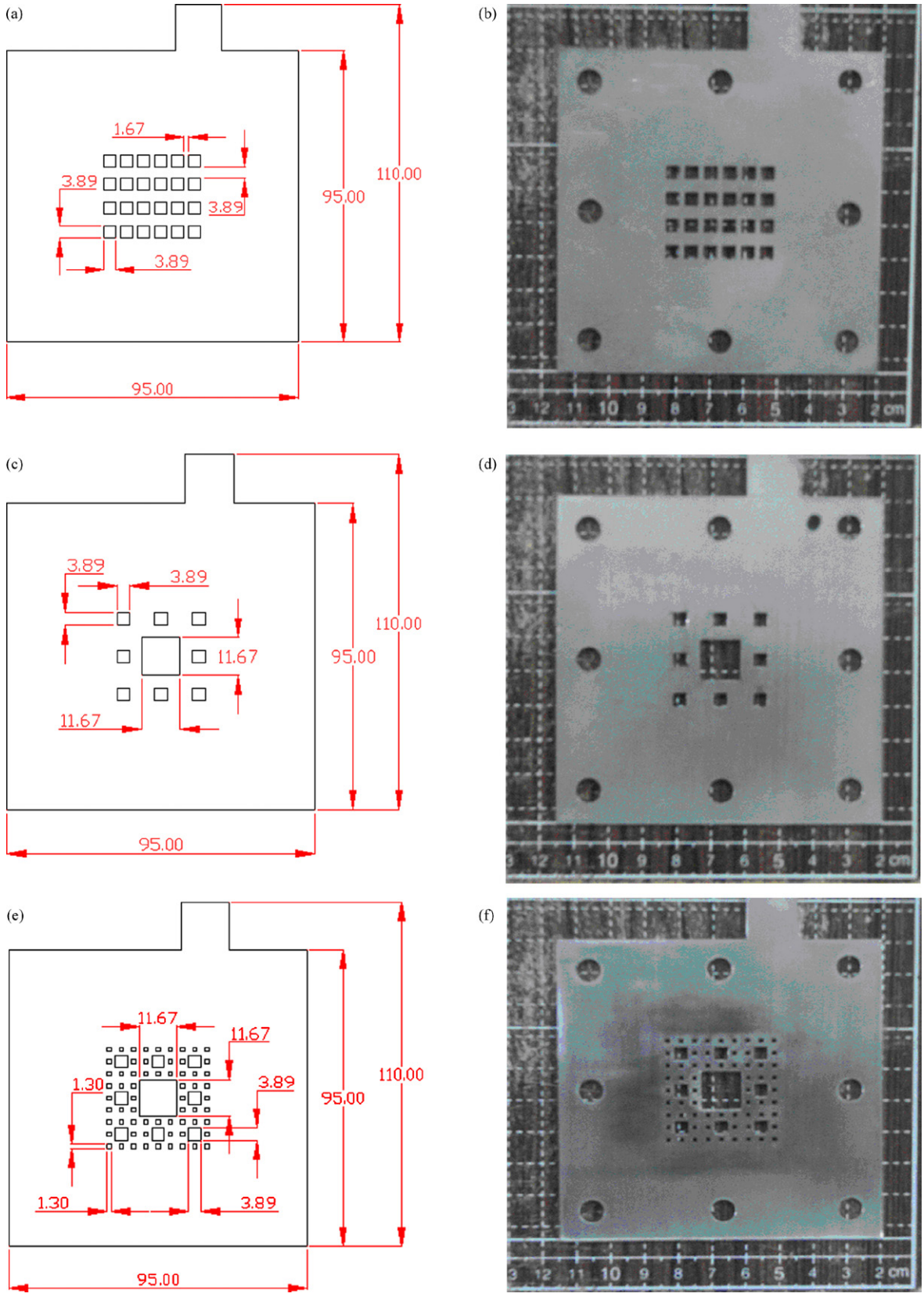

Fig. 5. Rectangular standard and Sirpsiski carpet fractal current collectors. (a) Standard rectangular current collector (SRCC). (b) Picture of SRCC. (c) 1st order rectangular fractal current collector (RFCC1). (d) Picture of RFCC1. (e) 2nd order rectangular fractal current collector (RFCC2). (f) Picture of RFCC2.

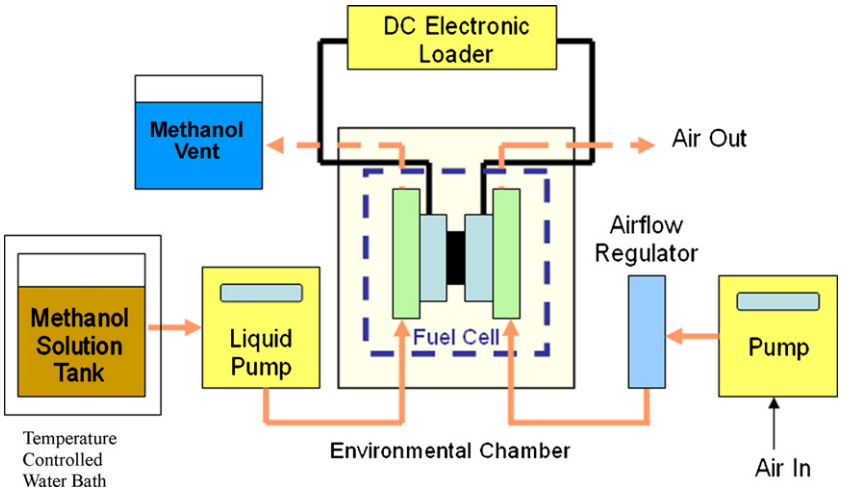

Fig. 6. Schematic illustration of the experimental setup.

2. Current collectors with Sierpinski carpets fractal holes

The fractal geometry theory is mathematically defined in the "Haussdorff dimensions", which are a set of non-integers. Many phenomena in nature, such as the patterns of clouds, the slope of valleys, or seashores, characterized by irregularity and chaos, can be described using the fractal geometry theory. It is difficult to describe these kinds of irregularities in very fine variation using conventional methods even via high order functions. The fractal geometry adopted in this research is the Sierpinski carpet. The Sierpinski carpet is a plane type fractal geometry that was advanced by Wacław Sierpiński in 1916. The Siepinski carpet starts with a solid square. This solid square is divided into 9 smaller congruent squares and the interior of the center square is removed. This is called the zero order of Siepinski carpets fractal. Each of the eight remaining solid squares are sub-divided into nine congruent squares and the center square from each is removed to obtain the first order Siepinski carpets fractal. This construction is repeated to obtain the second order Siepinski carpets fractal. The repeat procedure is called self-similarity in the theory of fractals. The proposed current collectors were constructed based on the Siepinski carpet fractal geometry and described as follows.

Table 1
Geometric information on current collectors with circular holes

Factors	Geometry		
	Standard	1st order fractal	2nd order fractal
Total perimeter length of holes (mm)	366.62	134.42	395.81
Total free open area (mm^2)	356.54	202.04	286.99
Total active MEA area (mm)	1225	1225	1225
Free open ratio (%)	29	16	23

Table 2
Geometric information of the current collectors with rectangular holes

Factors	Geometry		
	Standard	1st order fractal	2nd order fractal
Total perimeter length of holes (mm)	373.44	171.16	503.96
Total free open area (mm^2)	363.17	257.24	365.4
Total active MEA area (mm)	1225	1225	1225
Free open ratio (%)	29	21	30

2.1. Circular Sirpsiski carpet

For the circular Sirpsiski carpet geometry, the space is divided based on the following rules.

Let

n: the order of fractal geometry
N_n: the number of nth order open holes
D_n: The diameter of each nth order open hole
L: The length of the fractal domain side
A_n: Total area of nth order open hole
A_t: Total area of fractal open holes
L_t: Total perimeter length of the fractal open holes

Then

$$N_n = 8^{n-1} \tag{4}$$

$$D_n = 3^{-n-1}L \tag{5}$$

$$A_n = \left(\frac{\pi}{4}\right) D_n^2 N_n \tag{6}$$

$$A_t = \sum_{i=1}^{n} \left(\frac{\pi}{4}\right) D_i^2 N_i \tag{7}$$

$$L_t = \sum_{i=1}^{n} 2\pi D_i N_i \tag{8}$$

2.2. Rectangle Sirpsiski carpet

For the rectangle Sirpsiski carpet, the fractal rectangle geometry is divided based on the following rules.

Let

n: the order of fractal geometry
N_n: the number of nth order open holes
L_n: The diameter of each nth order open hole
L: The length of the fractal domain side
A_n: Total area of nth order open hole
A_t: Total area of fractal open holes
L_t: Total perimeter length of the fractal open holes

Table 3
Combination of anode and cathode current collector geometry

Experimental no.	Current collector with circle holes		Experimental no.	Current collector with rectangle holes	
	Anode	Cathode		Anode	Cathode
1–11	SCCC	SCCC	1–21	SRCC	SRCC
1–12	CFCC1	CFCC1	1–22	RFCC1	RFCC1
1–13	CFCC2	CFCC2	1–23	RFCC2	RFCC2
2–11	SCCC	SCCC	2–21	SRCC	SRCC
2–12	CFCC1	SCCC	2–22	RFCC1	SRCC
2–13	CFCC2	SCCC	2–23	RFCC2	SRCC
3–11	SCCC	SCCC	3–21	SRCC	SRCC
3–12	SCCC	CFCC1	3–22	SRCC	RFCC1
3–13	SCCC	CFCC2	3–23	SRCC	RFCC2

Then

$$N_n = 8^{n-1} \tag{9}$$

$$D_n = 3^{-n-1}L \tag{10}$$

$$A_n = L_n^2 N_n \tag{11}$$

$$A_t = \sum_{i=1}^{n} L_i^2 N_i \tag{12}$$

$$L_t = \sum_{i=1}^{n} 4L_i N_i \tag{13}$$

3. Experimental setup

This paper studies how the holes on the electric collector affect the DMFC performance using fractal and standard geometry. To

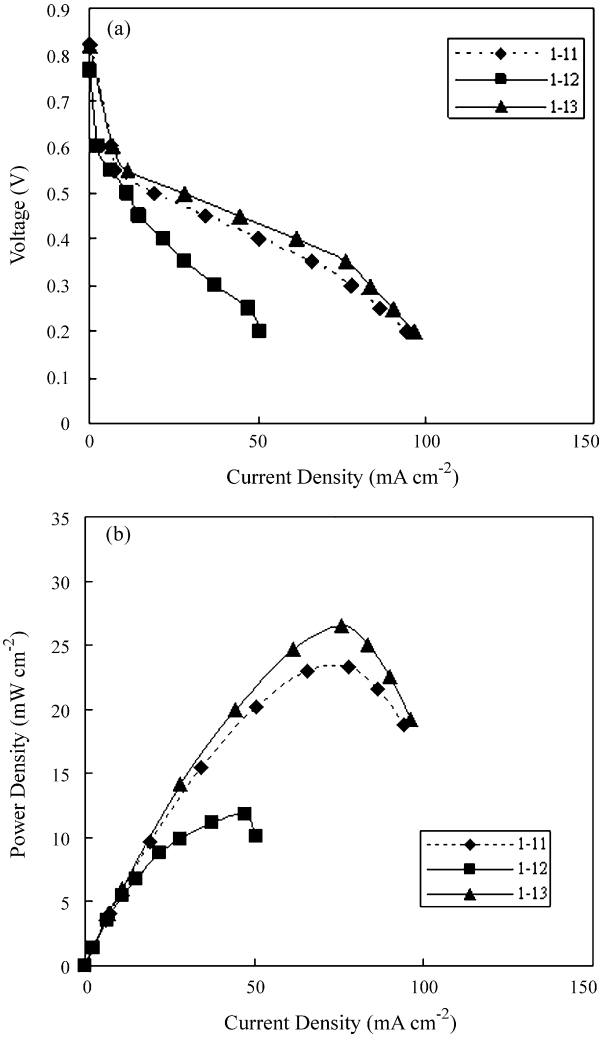

Fig. 7. Performance comparison of the DMFC with the same geometric configuration for the anode and cathode current collectors with circular holes under 15 cc min^{-1} anode flow rate. (a) *I–V* curves. (b) *I–P* curves.

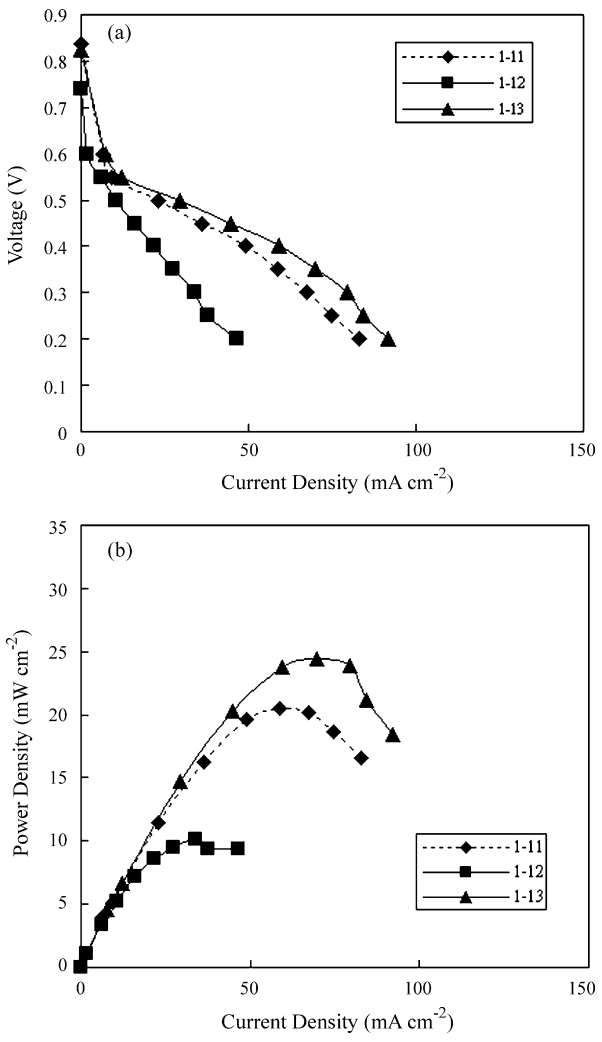

Fig. 8. Performance comparison of the DMFC with the same geometric configuration for the anode and cathode current collectors with circular holes under 10 cc min^{-1} anode flow rate. (a) *I–V* curves. (b) *I–P* curves.

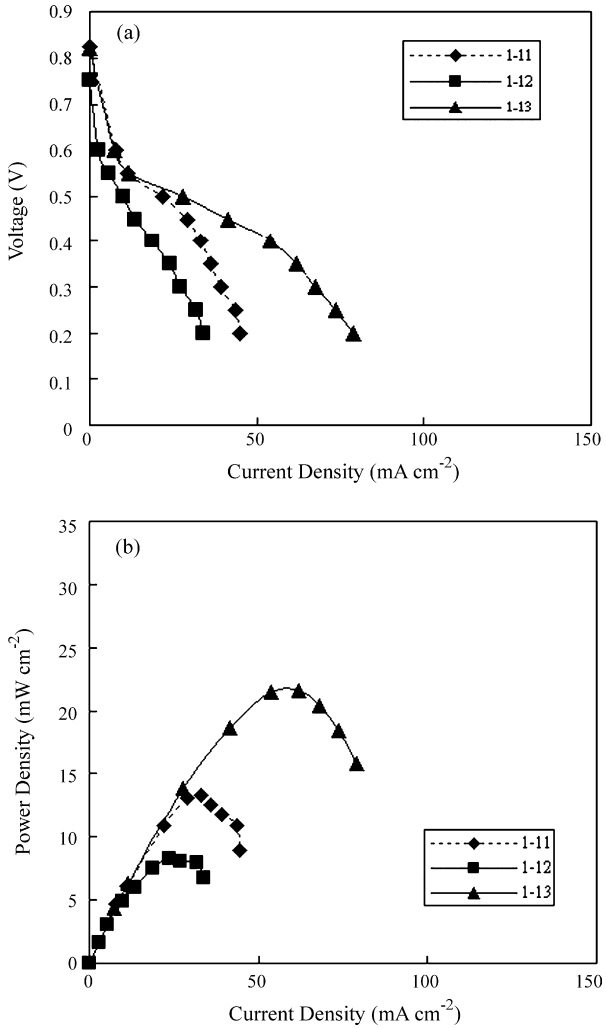

Fig. 9. Performance comparison of the DMFC with the same geometric configuration for the anode and cathode current collectors with circular holes under 5 cc min^{-1} anode flow rate. (a) *I–V* curves. (b) *I–P* curves.

simplify the experiments and ensure cell stability, a DMFC with stainless steel 316L (SS316L) current collectors was used to alternate the metal films on the PCB current collectors because SS316L has the advantages of easy machining, lower cost and good mechanical properties [16,17].

Fig. 3 shows the DMFC construction in Fig. 3(A). The anode and cathode flow boards are made of acrylic. Both the anode and cathode current collectors are made of SS316L. Each gasket is placed between the flow boards at the anode or cathode side. The complete assembly is shown in Fig. 3(B). The membrane electrode assembly (MEA) was sandwiched between the SS316L plates and used Nafion® 117 as the electrolyte with 4 mg cm^{-2} catalyst Pt-Ru catalytic loaded onto the anode and 4 mg cm^{-2} Pt-Ru loaded onto the cathode. The active size of a single cell in the experimental DMFC was 35 mm × 35 mm.

The current collectors were made of stainless steel with first and second order Sirpsiski carpet fractal holes. To make comparison, stainless steel current collectors with standard arranged circle and rectangle holes were also investigated. The detailed dimensions are illustrated as follows. The size of each current collector is 95 mm × 95 mm × 2 mm. The reactive area of the MEA is 35 mm × 35 mm. Fig. 4 shows the current collectors with a circular hole arrangement, including the standard circular current collector (SCCC) (Fig. 4a and b), the 1st order circular fractal current collector (CFCC1) (Fig. 4c and d), and the 2nd order Sirpsiski carpet circular current collector (CFBP2) (Fig. 4e and f). Fig. 5 shows the current collectors with the rectangular hole arrangement, including the standard rectangular current collector (SRCC) (Fig. 5a and b), the 1st order rectangular fractal current collector (RFCC1) (Fig. 5c and d), and the 2nd order rectangular fractal current collector (RFCC2) (Fig. 5e and f).

A schematic illustration of the experimental setup used in this research is shown in Fig. 6. The DMFC was placed into an environmental chamber and a methanol solution tank was placed in a temperature controlled water bath. The solution was preheated and pumped into the DMFC using a squirm liquid pump. The airflow was driven using an air pump with a flow regulator and pumped into the DMFC cathode. The DMFC was loaded using a DC electric loader. The data were recorded using a data acquisition (DAQ) system.

4. Results and discussion

In all experiments, the environmental conditions were kept at 55 °C temperature and 60% RH. The anode was supplied with a 2 M MeOH/DI water solution methanol at flow rates of 15 cc min^{-1} except those cases to show the consistency with different anode

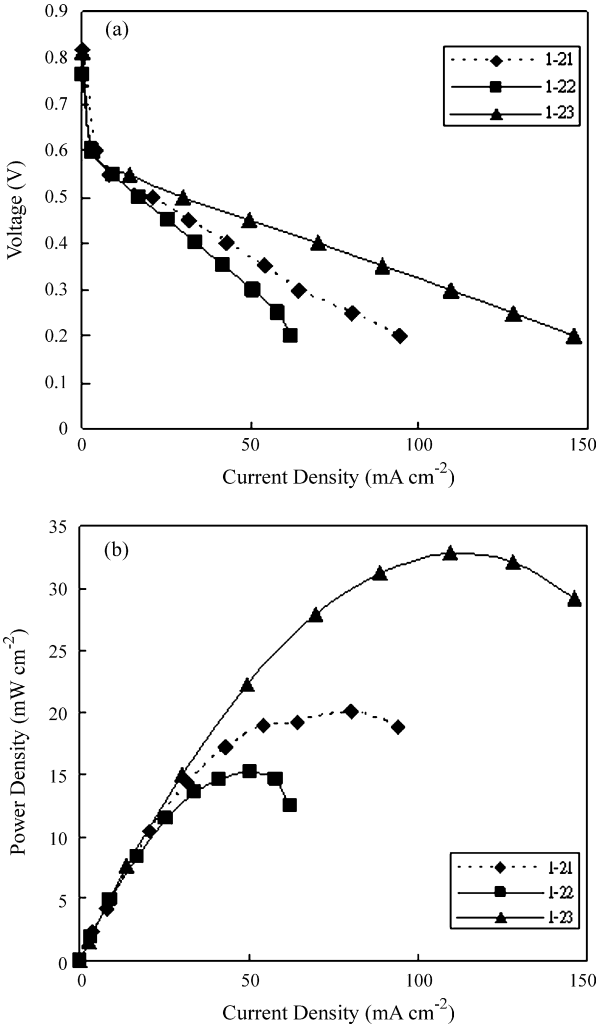

Fig. 10. Performance comparison of the DMFC with the same geometric configuration for the anode and cathode current collectors with rectangle holes under 15 cc min^{-1} anode flow rate. (a) *I–V* curves. (b) *I–P* curves.

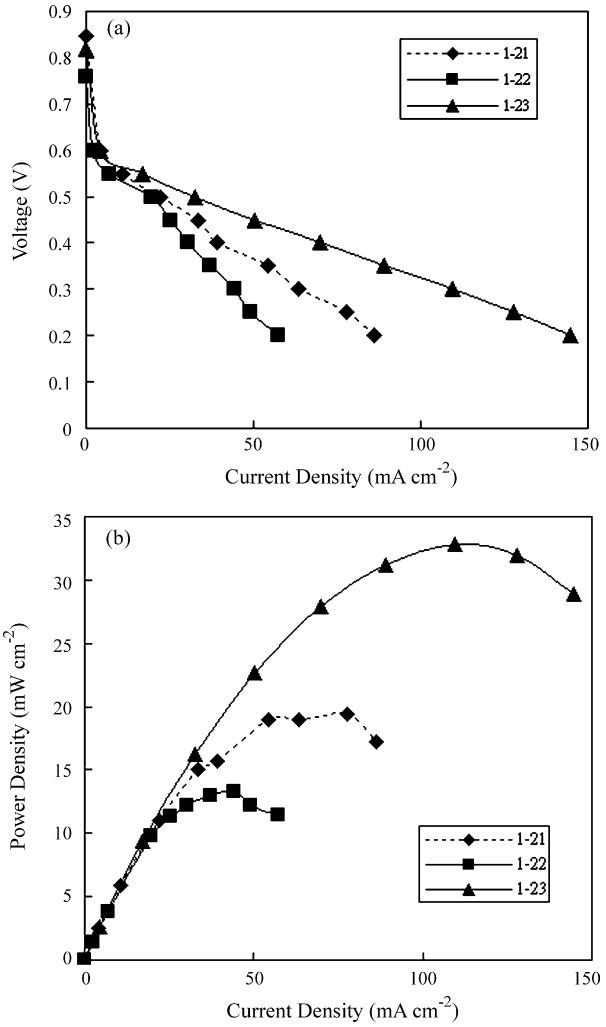

Fig. 11. Performance comparison of the DMFC with the same geometric configuration for the anode and cathode current collectors with rectangle holes under 10 cc min^{-1} anode flow rate. (a) *I–V* curves. (b) *I–P* curves.

flow rate in Section 4.1. The cathode side was fed air at a flow rate of 1000 cc min^{-1}. Table 1 shows the geometric information for the current collectors with circular holes. The total perimeter lengths with holes in the current collectors with the standard, 1st order fractal and 2nd order fractal circular holes were 366.62 mm, 134.42 mm, and 395.81 mm, respectively. The total free open areas in the current collectors with the standard, 1st order fractal and 2nd order fractal circular holes were 356.54 mm^2, 202.04 mm^2, and 286.99 mm^2, respectively. The free open ratios in the current collectors with the standard, 1st order fractal and 2nd order fractal circular holes were 29%, 16%, and 23%, respectively. Table 2 shows the geometric information for the current collectors with rectangular holes. The total perimeter length with holes in the current collectors with the standard, 1st order fractal and 2nd order fractal rectangle holes were 373.44 mm, 171.16 mm, and 503.96 mm, respectively. The total free open areas in the current collectors with the standard, 1st order fractal and 2nd order fractal rectangle holes were 363.17 mm^2, 257.24 mm^2, and 365.4 mm^2, respectively. The free open ratios in the current collectors with the standard, 1st order fractal and 2nd order fractal rectangle holes were 29%, 21%, and 30%, respectively. Table 3 shows the experimental number and the anode and cathode current collector combinations with various holes arrangements.

4.1. Same geometry configuration at anode and cathode

In this section, both the anode and cathode current collectors adopt the same geometric configuration. Figs. 7–9 are the performance comparison of DMFCs with the same anode and cathode current collectors with circular holes geometric configuration with 15 cc min^{-1}, 10 cc min^{-1} and 5 cc min^{-1} anode flow rate, respectively. Experiments number 1–11 represent DMFCs with standard circular current collectors at both the anode and cathode. Numbers 1–12 are DMFCs with 1st circular fractal current collectors at both the anode and cathode. Numbers 1–13 are DMFCs with 2nd circular fractal current collectors (CFCC2) at both the anode and cathode. The results show the same trend under different anode flow rates: The DMFC performance with CFCC2 is a little bit better than that for SCCC. The DMFC performance with CFCC1 is obviously lower. As shown in Table 1, CFCC2 has the longest total holes perimeter length, SCCC is second, and CFCC1 is shortest. The SCCC has the largest free open ratio, CFCC2 has the second, and CFCC1 has the smallest. Therefore, the short total holes perimeter length and small free open ratio lead to worse performance.

Figs. 10–12 shows a performance comparison of the DMFC with the same geometric configuration for the anode and cathode current collectors with rectangular holes. Experiments number 1–21

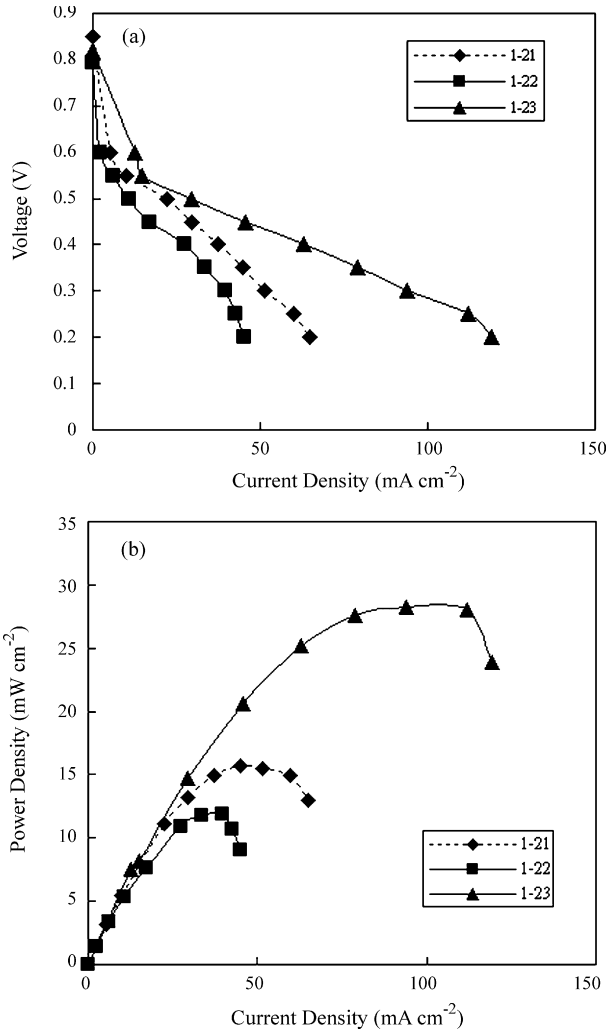

Fig. 12. Performance comparison of the DMFC with the same geometric configuration for the anode and cathode current collectors with rectangle holes under 5 cc min^{-1} anode flow rate. (a) *I–V* curves. (b) *I–P* curves.

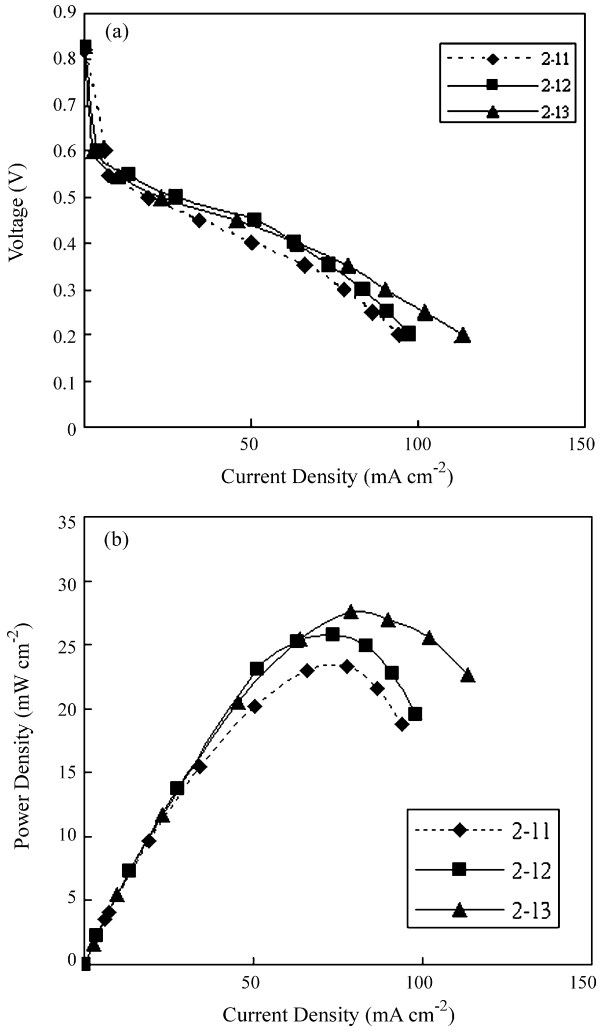

Fig. 13. Performance comparison of the DMFC with standard circular holes for the cathode current collector and an anode current collector with a different circular holes arrangement. (a) *I–V* curves. (b) *I–P* curves.

represent DMFCs with standard rectangle current collectors at both the anode and cathode with 15 cc min^{-1}, 10 cc min^{-1}, and 5 cc min^{-1} anode flow rate, respectively. Numbers 1–22 are DMFCs with 1st rectangular fractal current collectors at both the anode and cathode. Numbers 1–23 are DMFCs with 2nd rectangular fractal current collectors at both the anode and cathode. The results also show the same trend under different anode flow rates: the performance of the DMFC with RFCC2 is obviously better than SRCC, and the performance of the DMFC with RFCC1 is much lower. As shown in Table 2, the RFCC2 has the longest total holes perimeter length, SRCC has the second, and RFCC1 has the shortest. The RFCC2 has the largest free open ratio, SRCC has the second, and RFCC1 has the smallest. Similar to the circular case, the short total hole perimeter length and smaller free open ratio lead to worse performance. In addition, the DMFC shows better performance when the current collectors have rectangular holes than with circular holes at the same standard geometric order, 1st fractal order, and 2nd fractal order, i.e., SCCC > SRCC, RFCC1 > CFCC1, RFCC2 > CFCC2. Table 2 also shows that rectangular geometry has a longer total hole perimeter length and free open ratios at the same geometric order. As the results show the same trend under different anode flow rates, only the test results under 15 cc min^{-1} anode flow rate will be shown in the following studies to make the explanations brief.

4.2. Same geometry configuration at cathode but different at anode

This section studies the same geometry configuration is used at the cathode but different at the anode. Fig. 13 shows a performance comparison of the DMFC with standard circular holes in the cathode and anode current collectors with a different circular holes arrangement. Experimental numbers 2–11 represent DMFCs with standard circular current collectors at both the anode and cathode. Numbers 2–12 are DMFCs with a standard circular current collector at the cathode and 1st circular fractal current collector at the anode. Numbers 2–13 are DMFCs with a standard circular current collector at the cathode and 2nd circular fractal current collector at the anode. The results show that the cell performance order is CFCC2 > CFCC1 > SCCC, but the main differences occurs in the high current density range.

Fig. 14 shows a performance comparison of DMFCs with standard rectangular holes in the cathode current collector and an anode current collector with a different rectangular holes arrangement. Experiments number 2–21 represent DMFCs with standard rectangular current collectors at both the anode and cathode. Numbers 2–22 are DMFCs with a standard rectangular current collector at the cathode and a 1st rectangle fractal current collector at the anode. Numbers 2–23 are DMFCs with a standard rectangular

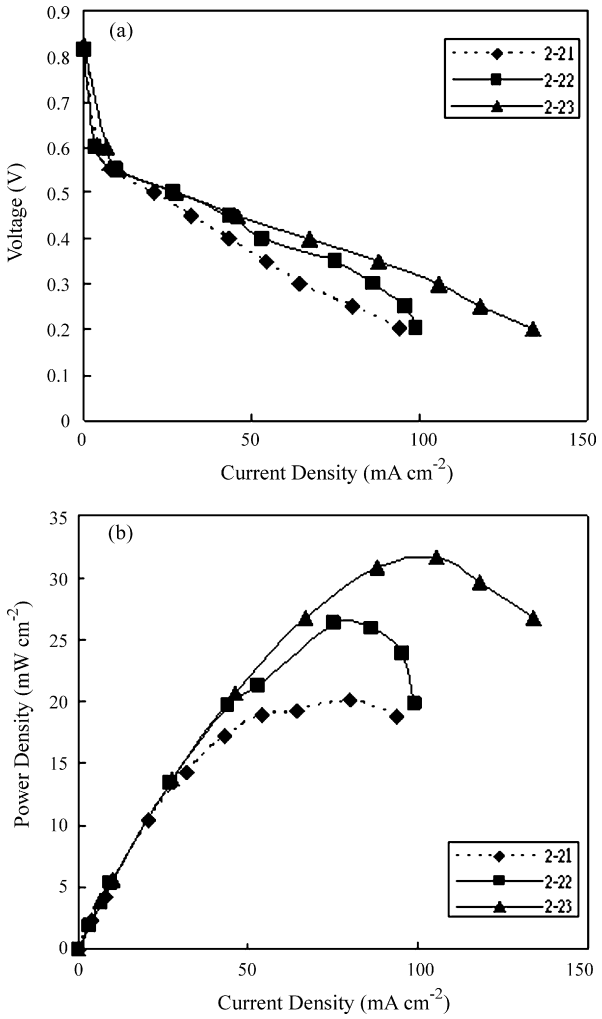

Fig. 14. Performance comparison of the DMFC with standard rectangle holes for the cathode current collector and an anode current collector with a different rectangular holes arrangement. (a) *I–V* curves. (b) *I–P* curves.

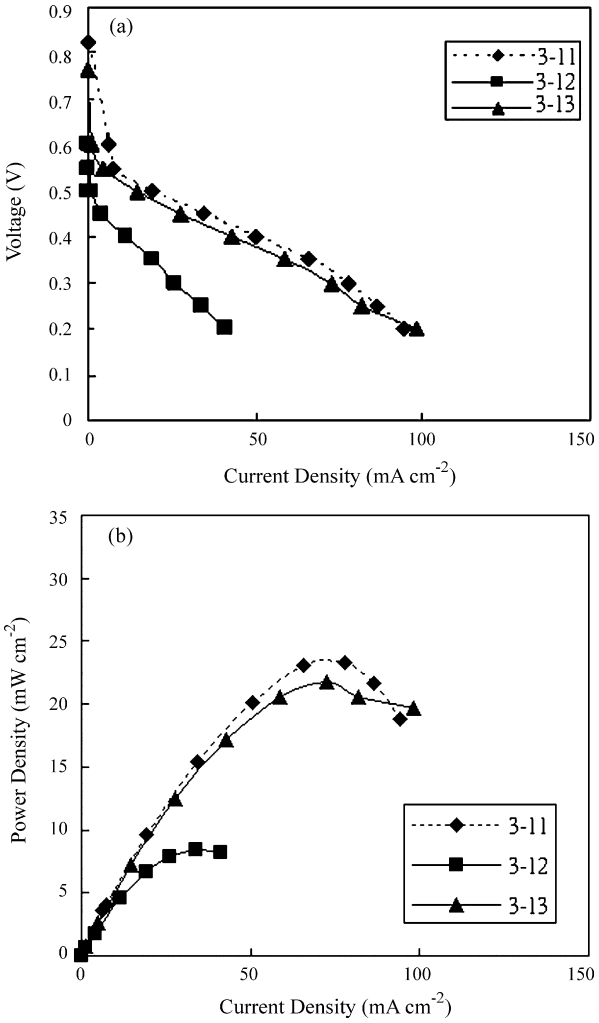

Fig. 15. Performance comparison of the DMFC with standard circular holes for the anode current collector and a cathode current collector with a different circular holes arrangement. (a) *I–V* curves. (b) *I–P* curves.

current collector at the cathode and a 2nd rectangle fractal current collector at the anode. The results show the cell performance order is RFCC2 > RFCC1 > SRCC. The differences among cells become larger than the circular cases.

4.3. Same geometry configuration at anode but different at cathode

In this section, same geometric configuration is used at the anode but different at the cathode. Fig. 15 shows a performance comparison of DMFCs with standard circular holes in the anode current collector and a cathode current collector with a different circular hole arrangement. Experiments number 3–11 represent DMFCs with standard circular current collectors at both the anode and cathode. Numbers 3–12 are DMFCs with a standard circular current collector at the anode and a 1st circular fractal current collector at the cathode. Numbers 3–13 are DMFCs with a standard circular current collector at the anode and a 2nd circular fractal current collector at the cathode. The results show that the DMFC performance with SCCC is a little bit better than that for CFCC2. The performance of the DMFC with CFCC1 is obvious lower. The CFCC2 has longest total holes perimeter length, SCCC has the second, and CFCC1 has the shortest. The SCCC has the largest free open ratio, CFCC2 has the second, and CFCC1 has the smallest. Moreover, the cathode current collector plays a significant role in the DMFC performance and the short total hole perimeter length and small free open ratio of the cathode current collector lead to worse performance.

Fig. 16 shows a performance comparison of DMFCs with standard rectangular holes in the anode current collector and a cathode current collector with a different rectangular hole arrangement. Experiments number 3–21 represent DMFCs with standard rectangular current collectors at both the anode and cathode. Numbers 3–22 are DMFCs with a standard rectangle current collector at the anode and a 1st rectangle fractal current collector at the cathode. Numbers 3–23 are DMFCs with a standard rectangular current collector at the anode and a 2nd rectangle fractal current collector at the cathode. Similar to the circular current collectors, the results are very close to the cases shown in Fig. 10. The results show that the DMFC performance with RFCC2 is obviously better than that for RFCC1. The performance of the DMFC with RFCC1 is much lower. The RFCC2 has the longest total hole perimeter length, SRCC has the second, and RFCC1 has the shortest. The RFCC2 has the largest free open ratio, SRCC has the second, and RFCC1 has the smallest. Similar to the rectangular case, the short total holes perimeter length and small free open ratio lead to worse performance. The DMFC showed better performance when the current collectors with the rectangular holes than circular holes in the same 1st fractal order and 2nd

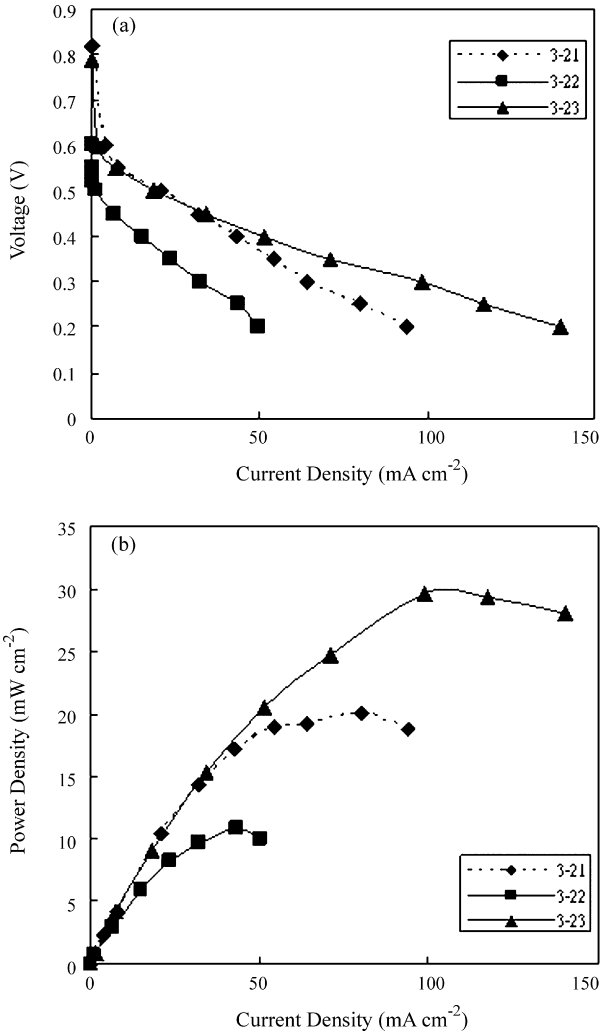

Fig. 16. Performance comparison of the DMFC with standard rectangular holes for the anode current collector and a cathode current collector with a different rectangular holes arrangement. (a) *I–V* curves. (b) *I–P* curves.

fractal order, i.e., RFCC1 > CFCC1, RFCC2 > CFCC2. Again, the cathode current collector played a significant role in the DMFC performance.

5. Conclusions

This paper presented a DMFC and current collectors with Sierpinski carpet fractal holes. The DMFC with the 2nd order fractal geometry showed better performance than current collectors with standard arranged holes. The cathode current collector effect was much greater than that for the anode current collector. Both the free open ratio and total hole perimeter length affected the cell performance, however, the total hole perimeter length yielded considerably more effect on DMFC performance than the free open hole ratio. Generally, longer total holes perimeter represented better cell performance, while shorter total perimeter length and free open hole ratio lead to poor cell performance. A longer total perimeter length under the same free open ratio is recommended for future current collectors design.

Acknowledgement

The authors would like to acknowledge the financial supports from National Science Council of Taiwan, ROC (NSC94-2212-E-149-004).

References

[1] Fuel Cell Handbook, fifth ed., E&G Services, Parson Inc., Science Applications International Corporation, 2000.
[2] G. Apanel, E. Johnson, Direct methanol fuel cells-ready to go commercial? Fuel Cells Bulletin (2004) 12.
[3] K. Scott, W.M. Taama, P. Argyropoulos, Engineering aspects of the direct methanol full cell system, Journal of Power Sources 79 (1999) 43.
[4] T. Schultz, S. Zhou, K. Sundmacher, Current status of and recent developments in the direct methanol fuel cell, Chemical Engineering Technology 24 (No. 12) (2001) 1223.
[5] H. Tsuchiya, O. Kobayashi, Mass production cost of PEM fuel cell by learning curve, International Journal of Hydrogen Energy 29 (2004) 985–990.
[6] A. Hermann, T. Chaudhuri, P. Spagnol, Bipolar plates for PEM fuel cells: a review, International Journal of Hydrogen Energy 39 (2005) 1297–1302.
[7] B.B. Mandelbrot, The Fractal Geometry of Nature, W.F. Freeman, San Francisco, 1982.
[8] D. Lee, W. Lin, Second law analysis on fractal-link fin under crossflow, Journal of AICHE 41 (1995) 2314–2317.
[9] G. Ledezma, A. Bejan, M. Errera, Contractual tree networks for heat transfer, Journal of Applied Physics 82 (1997) 89.
[10] D. Pence, Reduced pumping power and wall temperature in microchannel heat sinks with fractal-link branching channel networks, Microscale Thermophysical Engineering 6 (2002) 319–330.
[11] S. Lee, Y. Wang, C. Chen, Thermal performance of novel fractal heat sink fins, Journal of the Chinese Society of Mechanical Engineers 25 (2004) 547–556.
[12] C. Chen, Y. Juang, W. Lin, Generation of fractal toolpaths for irregular shapes of surface finishing areas, Journal of Materials Processing Technology 127 (2002) 146–150.
[13] K. Tuber, A. Oedegaard, M. Hermann, C. Hebling, Investigation of fractal flow-fields in portable proton exchange membrane and direct methanol fuel cells, Journal of Power Sources 131 (2004) 175–181.
[14] R. Crownover, Introduction to Fractals and Chaos, Jones and Bartlett Publishers, 1995.
[15] H. Peitgen, H. Jurgens, D. Saupe, Chaos and Fractals New Frontiers of Science, Springer-Verlag, 1992.
[16] R. Makkus, A. Jansseen, F. de Bruijn, R. Mallant, Stainless steel for cost-competitive bipolar plates in PEMFCs, Fuel Cells Bulletins 17 (2000) 5–9.
[17] J. Wind, R. Späh, W. Kaiser, G. Böhm, Metallic bipolar plates for PEM fuel cells, Journal of Power Sources 105 (2002) 256–260.